



Cite this: DOI: 10.1039/c8dt03964j

## A dual functional MOF-based fluorescent sensor for intracellular phosphate and extracellular 4-nitrobenzaldehyde†

Aniruddha Das,<sup>a</sup> Sourik Das,<sup>a</sup> Vishal Trivedi<sup>b</sup> and Shyam Biswas \*<sup>a</sup>

Herein, we present the successful synthesis, characterization and sensing application of a hydrazine functionalized Zr(IV)-based UiO-66 metal–organic framework (MOF) called Zr-UiO-66-N<sub>2</sub>H<sub>3</sub> (**1**). The guest-free material **1** shows selective and sensitive fluorimetric detection (turn-on mechanism) of phosphate (PO<sub>4</sub><sup>3-</sup>) anions in HEPES buffer (10 mM, pH = 7.4) and aqueous medium. It can also fluorimetrically detect (turn-off mechanism) 4-nitrobenzaldehyde (4-NB) in a HEPES:DMSO (9:1, v/v) medium with high selectivity and sensitivity. The selectivity for both analytes is retained in the presence of other potentially competitive analytes. The detection limit for PO<sub>4</sub><sup>3-</sup> ions is 0.196 μM, which is far below the PO<sub>4</sub><sup>3-</sup> level present in the aqueous environment. MOF **1** can detect intracellular phosphate and it also has the capacity to exhibit differences in the intracellular phosphate level. Furthermore, the probe is capable of sensing PO<sub>4</sub><sup>3-</sup> ions in real samples such as tap water, lake water, human urine and human blood serum. The sensitivity of the probe for sensing 4-NB is very high (detection limit = 4.7 μM). The possible mechanisms for sensing PO<sub>4</sub><sup>3-</sup> ions and 4-NB have been explored in detail by experimental techniques.

Received 2nd October 2018,  
Accepted 11th December 2018  
DOI: 10.1039/c8dt03964j

rsc.li/dalton

### Introduction

Phosphate (PO<sub>4</sub><sup>3-</sup>), being an inorganic anion, is a basic fragment of nucleotides and plays very vital roles in signal transduction and energy storage. The other important roles of this anion in biological systems include bone mineralization, muscle function, membrane robustness, cellular signaling, *etc.* The maximum permissible level of PO<sub>4</sub><sup>3-</sup> ions varies from 0.0143 to 0.143 mM for waste water and it is 0.32 μM for river water.<sup>1</sup> Excessive amounts of PO<sub>4</sub><sup>3-</sup> ions in food or water are often responsible for several digestive problems.<sup>2–4</sup> Because of their detrimental as well as favorable roles, the development of a practical method for the aqueous-phase detection of PO<sub>4</sub><sup>3-</sup> ions in an extremely selective and sensitive way will be beneficial for environmental protection as well as for human health.

On the other hand, chloramphenicol, which is extensively used as a first-line therapy for the treatment of typhoid fever patients and most commonly in eye drops (mainly in developing countries), gets decomposed in the presence of UV-A radiation of sunlight to produce various decomposition products such as 4-nitrobenzaldehyde (4-NB), 4-nitrobenzoic acid and 4-nitrosobenzoic acid.<sup>5</sup> The toxicities of all the three photo-products towards bone-marrow cells were studied, which concluded that 4-NB, 4-nitrobenzoic acid and 4-nitrosobenzoic acid were 20, 6 and 6 times more toxic than chloramphenicol, respectively.<sup>6</sup> Moreover, the use of this drug leads to an increased amount of methemoglobin (Met-Hb) in blood which is the cause of oxidative stress. Therefore, the *in vitro* sensing of 4-NB in a cell or in the fluid secreted from eyes being exposed to sunlight after the application of the eye drop is highly required, since it might be a prior indication of fatal aplastic anemia disease.<sup>7</sup>

Due to the unique structures and fascinating properties such as tunable and extraordinary porosity, high physico-chemical and mechanical stability and outstanding catalytic activity, metal–organic frameworks (MOFs) have received extensive research interest in recent years.<sup>8–10</sup> Besides gas storage, chemical catalysis,<sup>11,12</sup> chemical separation,<sup>13,14</sup> drug delivery,<sup>15,16</sup> and enzymatic catalysis,<sup>17–20</sup> MOFs have also been considered as one of the leading fluorescent sensor materials. Fluorescent MOFs have been used for the detection of a variety of organic and inorganic molecules, radicals, ions, *etc.*<sup>21–23</sup>

<sup>a</sup>Department of Chemistry, Indian Institute of Technology Guwahati, 781039 Assam, India. E-mail: sbiswas@iitg.ernet.in; Fax: +91-3612582349; Tel: +91-3612583309

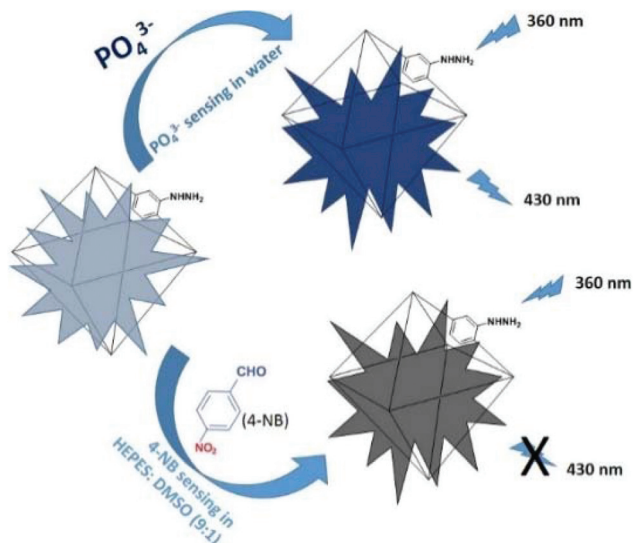
<sup>b</sup>Malaria Research Group, Department of Biosciences and Bioengineering, Indian Institute of Technology Guwahati, 781039 Assam, India

†Electronic supplementary information (ESI) available: Synthesis of ligands, mass spectra, NMR spectra, IR spectra, XRPD patterns, TG curves, N<sub>2</sub> sorption isotherms, fluorescence spectra, FE-SEM images, life-time decay profiles, table containing unit cell parameters of compound **1** and excited-state life-time values. See DOI: 10.1039/c8dt03964j

The choice of appropriate functional groups in the framework ligands is very crucial for the exhibition of sensing properties, since specific functional groups can act as binding sites for particular analytes, allowing their detection through fluorescence spectroscopy.

MOFs having high physicochemical stability (air, water, acid, base, thermal, *etc.*) are highly needed for their practical applications. The Zr(IV)-based MOF namely UiO-66 (UiO = University of Oslo) has received much attention in the past few years due to its high thermal and chemical stability as well as significant microporosity.<sup>24–28</sup> The 3D cubic framework of this MOF is constructed from  $[\text{Zr}_6\text{O}_4(\text{OH})_4]^{12+}$  building units, which are interconnected by the carboxylate groups of 1,4-benzenedicarboxylate (BDC) ligands.<sup>29</sup> In compound **1**, the BDC ligand molecules are replaced by the 2-hydrazinyl-1,4-benzenedicarboxylate (BDC- $\text{N}_2\text{H}_3$ ) ligands. The guest-free form of **1** (termed **1'**) can sense  $\text{PO}_4^{3-}$  ions in water and HEPES buffer (10 mM, pH = 7.4). It can also detect 4-NB in the HEPES (10 mM, pH = 7.4)/DMSO (v/v, 9:1) medium. The detection processes for both analytes occur with high selectivity, which is preserved in the presence of intrusive analytes (Scheme 1). Herein, we report the highly selective and sensitive fluorescence sensing properties of **1'** for  $\text{PO}_4^{3-}$  ions and 4-NB *via* turn-on and turn-off mechanisms, respectively.

In addition to its high physicochemical stability, a Zr-based MOF was chosen for the sensing of  $\text{PO}_4^{3-}$  ions due to the high binding affinity of Zr(IV) ions with  $\text{PO}_4^{3-}$  ions. There is already a report in the literature on  $\text{PO}_4^{3-}$  sensing by a Zr-based MOF.<sup>30</sup> Moreover, the Zr(IV) ions having a  $d^0$  electronic configuration are electronically inert. Hence, there is good electronic communication between the Zr(IV) ions and BDC- $\text{N}_2\text{H}_3$  ligands.<sup>31,32</sup> As a result, **1'** showed a high fluorescence intensity.



**Scheme 1** Schematic representation displaying the sensing properties of **1'** towards  $\text{PO}_4^{3-}$  ions in aqueous medium and 4-NB in the HEPES/DMSO (v/v, 9:1) medium through fluorescence turn-on and turn-off mechanisms, respectively.

## Experimental

### Materials and general methods

The 2-hydrazinyl-1,4-benzenedicarboxylic acid ( $\text{H}_2\text{BDC}-\text{N}_2\text{H}_3$ ) ligand was synthesized by following the previously reported procedure<sup>33</sup> for 2-hydrazinyl-4-(methoxycarbonyl) benzoic acid. The synthesis and characterization (Fig. S1–S3†) of the ligand are presented in the ESI.† All the chemicals used in this work were commercially available and they were used without any further purification. For fluorescence sensing experiments Milli-Q water was used as a medium. Fourier transform infrared spectroscopy was performed in the region 400–4000  $\text{cm}^{-1}$  with a PerkinElmer Spectrum Two FT-IR spectrometer. The following indications were used to indicate the corresponding absorption bands: very strong (vs), strong (s), medium (m), weak (w), shoulder (sh) and broad (br). Thermogravimetric analyses (TGA) were carried out using a SDT Q600 thermogravimetric analyzer in the temperature range 25–700 °C under an argon atmosphere at a heating rate of 10 °C  $\text{min}^{-1}$ . A Bruker D2 Phaser X-ray diffractometer (30 kV, 10 mA) using  $\text{Cu}-\text{K}\alpha$  ( $\lambda = 1.5406 \text{ \AA}$ ) radiation was used to obtain the X-ray powder diffraction (XRPD) patterns. An Edinburgh Instrument Life-Spec II equipment was used to measure the fluorescence lifetimes (TRPL) by employing the time-correlated single-photon counting (TCSPC) procedure. The solution  $^1\text{H}$  and  $^{13}\text{C}$  NMR spectra were recorded on a Bruker AM 600 spectrometer. Nitrogen sorption isotherms were recorded on a Quantachrome Autosorb iQMP gas sorption analyzer. Fluorescence emission studies were performed using a HORIBA JOBIN YVON Fluoromax-4 spectrofluorometer. The compound was heated at 120 °C for 24 h before the sorption experiments.

### Synthesis of $[\text{Zr}_6\text{O}_4(\text{OH})_4(\text{BDC}-\text{N}_2\text{H}_3)_6]\cdot 3.5\text{H}_2\text{O}\cdot 3\text{DMF}$ (Zr-UiO-66- $\text{N}_2\text{H}_3$ , **1**)

A mixture of  $\text{ZrOCl}_2\cdot 8\text{H}_2\text{O}$  (65 mg, 0.20 mmol),  $\text{H}_2\text{BDC}-\text{N}_2\text{H}_3$  ligand (40 mg, 0.20 mmol) and benzoic acid (746 mg, 6.0 mmol) in 3 mL of *N,N*-dimethylformamide (DMF) was sealed in a glass tube and heated using a block heater at 120 °C for 24 h. The light yellow precipitate was collected by vacuum filtration and washed with acetone ( $2 \times 3 \text{ mL}$ ). The material was dried at 60 °C for 4 h in a conventional oven. The yield was 45 mg (0.02 mmol, 60%) based on the Zr salt. FT-IR (KBr,  $\text{cm}^{-1}$ ): 3420 (br), 2916 (w), 2853 (w), 1658 (s), 1627 (vs), 1422 (s), 1418 (vs), 1381 (m), 1188 (m), 1100 (w), 1028 (m), 900 (m), 880 (sh), 845 (s), 782 (vs), 711 (sh), 663 (vs), 558 (w), 495 (s).

### Activation of the compound

To obtain the activated form, 50 mg of the as-synthesized compound was stirred for 24 h in 30 mL of methanol in a round-bottom flask at room temperature, during which fresh methanol was added discarding the initially added methanol at a time interval of 12 h. After that the compound was filtered and the solid powder was dried at 80 °C in a conventional oven for 1 h. After that, the compound was heated at 120 °C under vacuum for 24 h to obtain material **1'**.

### Preparation of the suspensions of **1'** for fluorescence sensing experiments

To obtain stable suspensions for the luminescence detection experiments, 2 mg of **1'** was taken in three separate 5 mL glass vials. Then, 3 mL of water, HEPES (10 mM, pH = 7.4) (the first two for PO<sub>4</sub><sup>3-</sup> sensing) or a HEPES (10 mM, pH = 7.4)/DMSO (v/v = 9 : 1) mixture (for 4-NB sensing) was separately added to these vials. These mixtures were allowed to sonicate for 1 h and subsequently kept for 24 h under ambient conditions.

### Fluorescence sensing experiments

In order to perform the sensing experiment for PO<sub>4</sub><sup>3-</sup> ions, 100 μL of the suspension of **1'** from the stock suspension was placed in a quartz cuvette and 2900 μL of water or HEPES buffer was added to it in order to make a suspension having a total volume of 3 mL. Then, a solution of PO<sub>4</sub><sup>3-</sup> ions was added to it up to 400 μL with an incremental volume of 50 μL and the emission spectra were recorded after every 5 or 10 min until the fluorescence intensity reached the saturation point. For the sensing of 4-NB, 100 μL of the suspension of **1'** from the stock suspension was taken in a quartz cuvette and 2900 μL of the HEPES/DMSO (v/v = 9 : 1) mixture was added to it in order to make a suspension having a total volume of 3 mL. Then, a solution of 4-NB in DMSO was added to it up to 400 μL with an incremental volume of 50 μL and the fluorescence spectra were recorded until the saturation point for the fluorescence intensity was attained. For all these cases, the suspension of **1'** was excited at 360 nm and the fluorescence spectra were recorded in the range of 385–585 nm. The fold increment for the PO<sub>4</sub><sup>3-</sup> sensing *via* the turn-on mechanism was calculated using the formula: fold increment =  $(I/I_0 - 1)$ . The quenching efficiency ( $\eta$ ) for the 4-NB sensing was calculated using the familiar equation:  $\eta = (1 - I/I_0) \times 100\%$ , where  $I_0$  is the initial fluorescence intensity of the suspension of **1'** and  $I$  is the fluorescence intensity after the addition of the analyte.

### Cell culture and intracellular PO<sub>4</sub><sup>3-</sup> sensing

The macrophage J774A.1, cervical cancer HeLa and glioblastoma U87MG cells were cultured in DMEM:F12 media containing 10% FBS and 1% antibiotic cocktails as described earlier.<sup>34–36</sup> The cells were loaded with probe **1'** (0.5 mg mL<sup>-1</sup>) for 6 h in complete medium. The cells were observed in the bright field and the blue channel ( $\lambda_{\text{ex}} = 390$  nm,  $\lambda_{\text{em}} = 430$  nm) using the Cytell cell imaging system (GE Healthcare) and images were captured from randomly selected fields.

### PO<sub>4</sub><sup>3-</sup> sensing in real samples

We analyzed PO<sub>4</sub><sup>3-</sup> ions in six different types of real samples: tap and lake water (collected locally), urine 1 and 2 (collected from two different human volunteers), and blood serum 1 and serum 2 (collected from two different human volunteers). Human urine samples were kept at 4 °C overnight and then the supernatant liquid was collected which was used for the sensing experiment. Human serum samples were centrifuged

at 5000 rpm for 5 min and then filtered with Amicon® Ultra-4 Centrifugal Filter Units (30 kDa). The filtrate was collected which was diluted 100 times with HEPES buffer (10 mM, pH = 7.4). The resulting liquid was used for the sensing experiment. These samples were distributed in twenty four glass vials so that four vials contain samples of one type. After that, a known amount of Na<sub>3</sub>PO<sub>4</sub> was spiked into every vial so that the final concentration of PO<sub>4</sub><sup>3-</sup> ions in four different glass vials having samples of one kind become 0, 10, 20 and 30 μM. Then, each PO<sub>4</sub><sup>3-</sup> spiked sample (100 μL) was added to the aqueous suspension (2900 μL) of **1'**. We recorded the fluorescence spectrum after 100 min of addition.

## Results and discussion

### Preparation and activation procedure

Before determining the optimized synthesis conditions for **1**, several possible reactions were carried out with the H<sub>2</sub>BDC-N<sub>2</sub>H<sub>3</sub> ligand using three Zr(IV) salts (ZrCl<sub>4</sub>, ZrOCl<sub>2</sub>·8H<sub>2</sub>O) in the presence of two different amide solvents (*N,N*-dimethylformamide, *N,N*-dimethylacetamide) and four different modulators (acetic acid, formic acid, benzoic acid and trifluoroacetic acid)<sup>37</sup> at different temperatures. Highly crystalline compound **1** was obtained when a mixture of ZrOCl<sub>2</sub>·8H<sub>2</sub>O, H<sub>2</sub>BDC-N<sub>2</sub>H<sub>3</sub> ligand and benzoic acid was placed in DMF in a sealed glass tube and heated at 120 °C for 24 h using a block heater.

In order to remove the guest molecules trapped inside the pores of **1**, an activation procedure was performed which involves a solvent-exchange step followed by a heating step under high vacuum. In the solvent-exchange step, 100 mg of **1** was suspended in 30 mL of methanol inside a 50 mL round-bottom flask and stirred for 24 h at room temperature. Then, it was filtered and dried at 60 °C in a conventional oven. Furthermore, it was activated at 120 °C under vacuum for 24 h.

### Infrared spectroscopy

In the FT-IR spectra (Fig. S4, ESI†) of the as-synthesized **1** and activated **1'**, the strong absorption bands at around 1570 and 1400 cm<sup>-1</sup> can be attributed to the asymmetric and symmetric carboxylate stretching vibrations of the coordinated BDC-N<sub>2</sub>H<sub>3</sub> ligand molecules, respectively.<sup>38</sup> In the IR spectrum of the as-synthesized sample, the strong absorption band at 1658 cm<sup>-1</sup> can be attributed to the carbonyl stretching vibration of the occluded DMF molecules in the framework structure.<sup>39</sup> This absorption band is completely absent in the FT-IR spectrum of **1'**, which confirms that the thermally activated compound is devoid of any guest DMF molecule inside the pores.

### XRPD analysis

The experimental XRPD patterns (Fig. 1) of **1** and **1'** match nicely with the simulated XRPD pattern of the previously reported UiO-66 compound.<sup>40,41</sup> By indexing the XRPD pattern of **1**, its unit cell parameters were deduced. The observed lattice parameters (Table S1, ESI†) are very close to the

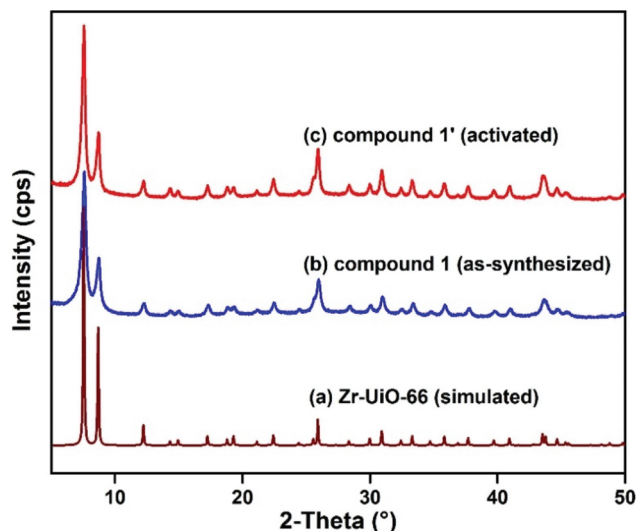


Fig. 1 XRPD patterns of the (a) simulated Zr-UiO-66, (b) as-synthesized **1** and (c) activated **1'**.

reported, un-functionalized Zr-UiO-66 compound. In addition, a Pawley fit (Fig. S5, ESI†) was carried out, which displayed very good similarity between the experimental and calculated XRPD patterns of **1**. All these results suggest that the presented compound has the same framework topology as the UiO-66 material.<sup>40</sup>

The noticeable similarity between the XRPD patterns of the as-synthesized and thermally activated samples of **1** indicates that the compound retained its structural robustness after the thermal activation process. We also obtained the XRPD patterns of **1'** after the fluorescence sensing (for phosphate and 4-NB) measurements. The XRPD patterns displayed in Fig. S6 (ESI†) disclose that the crystallinity and hence the structural integrity of the material remain unaltered after the fluorescence sensing measurements. These results suggest that **1'** is a very effective potential material for real-world sensing applications.

### Structure description

As confirmed by the XRPD experiments (Fig. 1), the hydrazine-functionalized Zr(IV)-based UiO-66 material (**1**) shows the same framework topology as the un-functionalized UiO-66 material. Lillerud and co-workers have previously described the framework structure of the UiO-66 material.<sup>42</sup> The UiO-66 framework contains hexanuclear  $[\text{Zr}_6\text{O}_4(\text{OH})_4]^{12+}$  bricks as the secondary building units which are interlinked by the carboxylates of twelve 1,4-benzenedicarboxylate (BDC) ligands. In the presented work, BDC- $\text{N}_2\text{H}_3$  plays the same role as the BDC ligand in the previously reported<sup>42,43</sup> UiO-66 framework structure. This 3D framework contains octahedral as well as tetrahedral cages. Each central octahedral cage is connected by eight corner tetrahedral cages *via* narrow triangular windows. Each zirconium atom resides in a square anti-prismatic coordination environment of the framework. The organic connector

and the inorganic building units together make the framework three-dimensional *via* the interconnection with each other.

### Thermal stability

For investigating the thermal stability of **1** and **1'**, thermogravimetric (TG) analyses were performed under an argon atmosphere in the temperature range of 25–700 °C. According to the TG analyses, **1** is thermally stable up to 400 °C under the air atmosphere.

In the TG curve (Fig. S7, ESI†) of **1**, the first loss of 2.6 wt% in the temperature range of 25–120 °C can be attributed to the elimination of 3.5 water molecules per formula unit (calcd: 2.5 wt%). The second weight loss of 12.2 wt% in the temperature range of 120–400 °C can be assigned to the removal of 3 occluded DMF molecules per formula unit (calcd: 11.8 wt%). After 400 °C, the decomposition of the compound starts to occur owing to the loss of organic ligands from the framework structure of **1**. In the TG trace of **1'**, the one weight loss in the low temperature range can be assigned to the removal of adsorbed water molecules from moisture. It is worth noting that the thermal stability of our compound **1'** is lower than the existing, parent and functionalized Zr-based UiO-66 MOF materials.<sup>44–46</sup>

### Chemical stability

The chemical stability of **1'** was investigated by stirring the samples in water, acetic acid and 1M HCl solutions at room temperature for 12 h. After that, the samples were collected by filtration and the crystallinity of the filtered materials was checked by XRPD analysis. As shown in Fig. S6, ESI†, the compound retained its crystallinity (and thus structural robustness) after treatment with water, acetic acid and 1M HCl solutions. Hence, **1'** exhibited remarkable chemical stability which is comparable to that of the previously reported parent and other functionalized UiO-66 materials.<sup>47</sup>

### N<sub>2</sub> sorption analysis

The N<sub>2</sub> sorption experiments were carried out for the determination of the specific surface area and the micropore volume of **1'**. From Fig. S8 (ESI†), it is obvious that the N<sub>2</sub> adsorption isotherm follows type-I behavior, which is characteristic of microporous materials. The BET surface area and micropore volume of **1'** were estimated to be 818 m<sup>2</sup> g<sup>-1</sup> and 0.47 cm<sup>3</sup> g<sup>-1</sup> (at  $p/p_0 = 0.5$ ), respectively. This value of the BET surface area is comparable to the known, functionalized UiO-66 MOF materials.<sup>48–54</sup>

We also performed N<sub>2</sub> sorption measurements (Fig. S9, ESI†) with the compound recovered after the phosphate sensing experiment. As anticipated, the BET surface area and micropore volume (at  $p/p_0 = 0.5$ ) of the phosphate-treated material were lower than the untreated material and they corresponded to 442 m<sup>2</sup> g<sup>-1</sup> and 0.25 cm<sup>3</sup> g<sup>-1</sup>, respectively.

### Photoluminescence properties of **1'**

We studied the solid-state fluorescence properties of both the free H<sub>2</sub>BDC- $\text{N}_2\text{H}_3$  ligand and **1'**. The free H<sub>2</sub>BDC- $\text{N}_2\text{H}_3$  ligand

displayed a weak fluorescence intensity ( $\lambda_{\max} = 447 \text{ nm}$ ) and **1'** exhibited a strong luminescence intensity ( $\lambda_{\max} = 478 \text{ nm}$ ) in the solid state (Fig. S10, ESI†). The fluorescence emission band of the free ligand arises due to the  $\pi\text{-}\pi^*$  electronic transition of the aromatic ring.<sup>55</sup> The enhanced luminescence intensity of **1'** as compared to the free ligand can be assigned to the ligand-to-metal charge transfer (LMCT).<sup>56,57</sup> The blue shift in the  $\lambda_{\max}$  value of **1'** as compared to the free ligand might also be assigned to the LMCT transition.<sup>58,59</sup>

We also investigated the luminescence properties of both the free  $\text{H}_2\text{BDC-N}_2\text{H}_3$  ligand and **1'** in the aqueous medium. The free ligand showed a strong luminescence intensity ( $\lambda_{\max} = 443 \text{ nm}$ ) and **1'** exhibited a weak luminescence intensity ( $\lambda_{\max} = 458 \text{ nm}$ ) in the aqueous medium (Fig. S10, ESI†). This difference in the luminescence intensity can be ascribed to the interaction between the Zr–O nodes and water molecules. When water molecules enter inside the pores of **1'**, they can form hydrogen bonding with the Zr–O nodes of **1'** and thus perturb the electron transfer from the ligand to metal (*i.e.*, LMCT transition).<sup>60</sup> This perturbation reduces the luminescence intensity of **1'** in the aqueous medium.

### Sensing behavior towards $\text{PO}_4^{3-}$ ions

In order to determine the potential of UiO-66- $\text{N}_2\text{H}_3$  as a fluorogenic sensor for  $\text{PO}_4^{3-}$  detection in the aqueous or HEPES buffer medium, fluorescence titration experiments were performed with the suspension of **1'**. The fluorescence emission ( $\lambda_{\text{ex}} = 360 \text{ nm}$ ) spectra of the suspension of **1'** were recorded in the range of 385–585 nm upon gradual addition (50  $\mu\text{L}$  for each addition) of 2 mM  $\text{PO}_4^{3-}$  solution. The fluorescence emission intensities were regulated at 430 nm. As shown in Fig. 2, the saturation of the fluorescence intensity was observed after the addition of 400  $\mu\text{L}$  of the 2 mM  $\text{PO}_4^{3-}$  solution to the aqueous suspension of **1'**. Further addition of the  $\text{PO}_4^{3-}$  solu-

tion did not result in any considerable increment in the fluorescence intensity.

The detection performance of **1'** towards  $\text{PO}_4^{3-}$  ions was evaluated by performing time-dependent sensing experiments. Upon the addition of 400  $\mu\text{L}$  of the 2 mM  $\text{PO}_4^{3-}$  solution, the fluorescence emission spectra of **1'** (in both aqueous and HEPES buffer media) were recorded at a regular time interval of 10 min until the saturation in the fluorescence emission intensity was attained. The addition of the  $\text{PO}_4^{3-}$  solution to the suspension of **1'** led to the gradual transformation of the compound into a turn-on state from its initial turn-off state. The saturation in the fluorescence emission intensity of **1'** occurred after 90 and 100 min in aqueous (Fig. 3) and HEPES (Fig. S11, ESI†) buffer media, respectively. Therefore, the compound is a potential fluorescent turn-on probe for the detection of  $\text{PO}_4^{3-}$  ions under both aqueous and physiological conditions.

The high selectivity of a sensor towards  $\text{PO}_4^{3-}$  ions over other potentially competing anions is very crucial for practical applications. Hence, we measured the fluorescence turn-on response of **1'** (in both water and 10 mM HEPES buffer) towards various potentially interfering inorganic anions and organic molecules containing  $\text{PO}_4^{3-}$  ions such as NaCl, NaBr, NaF,  $\text{NaH}_2\text{PO}_4$ ,  $\text{Na}_2\text{HPO}_4$ ,  $\text{Na}_3\text{P}_2\text{O}_7$ , NaI,  $\text{NaNO}_2$ ,  $\text{NaNO}_3$ , NaOAc,  $\text{Na}_2\text{S}$ ,  $\text{Na}_2\text{SO}_4$ , NaHS, NaCN,  $\text{NaHCO}_3$ ,  $\text{NaClO}_4$ , NaSCN, adenosine diphosphate (ADP) and adenosine triphosphate (ATP). It can be seen from Fig. 4 and Fig. S12–S13 (ESI†) that the addition of an inorganic  $\text{PO}_4^{3-}$  solution to the suspension of **1'** causes a dramatic increment in the fluorescence emission intensity. In the presence of all the other possibly competing anions, there was almost negligible enhancement in the fluorescence emission intensity as compared to the  $\text{PO}_4^{3-}$  anion. These results suggest that the fluorescent turn-on probe is highly selective towards  $\text{PO}_4^{3-}$  ions over other potentially interfering anions.

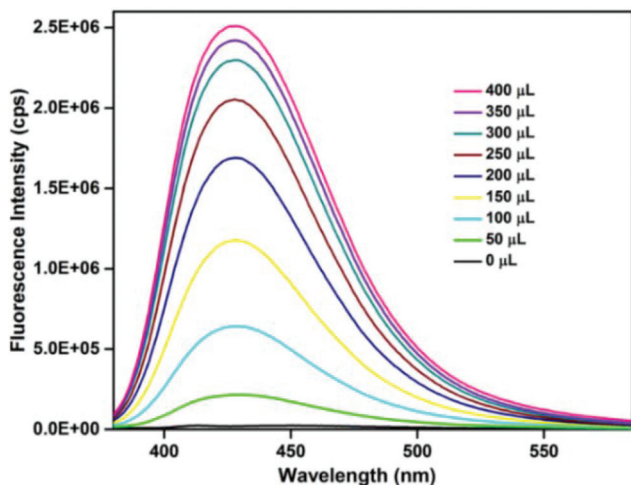


Fig. 2 Enhancement of the fluorescence intensity of **1'** (0.87 mM) upon gradual addition of 400  $\mu\text{L}$  of the 2 mM aqueous solution of  $\text{PO}_4^{3-}$  ions ( $\lambda_{\text{ex}} = 360 \text{ nm}$ ,  $\lambda_{\text{em}} = 430 \text{ nm}$ ).

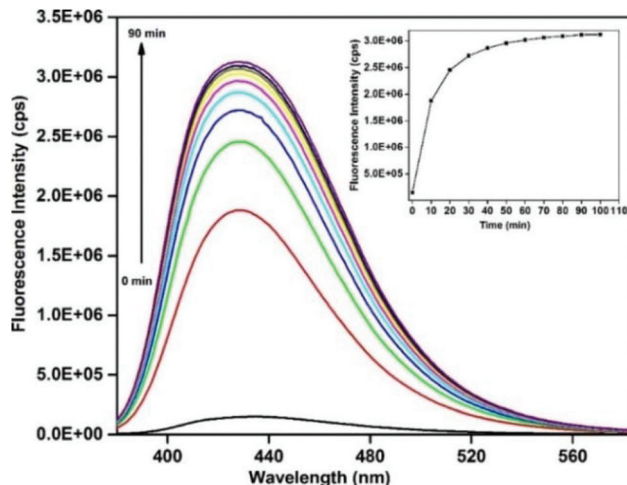


Fig. 3 Enhancement of the fluorescence intensity of **1'** (0.87 mM) with time upon addition of 400  $\mu\text{L}$  of the 2 mM aqueous solution of  $\text{PO}_4^{3-}$  ions ( $\lambda_{\text{ex}} = 360 \text{ nm}$ ,  $\lambda_{\text{em}} = 430 \text{ nm}$ ).

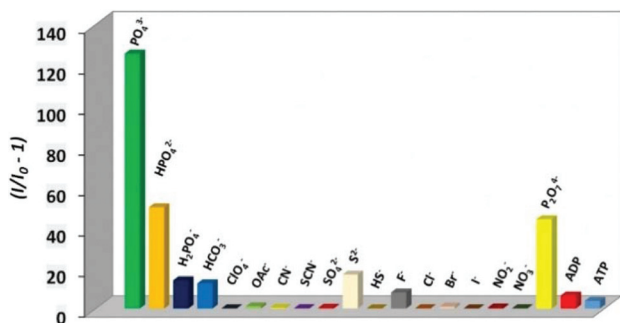


Fig. 4 Change in the fluorescence intensity of the suspension of **1'** (0.87 mM) upon the addition of 400  $\mu\text{L}$  of 2 mM aqueous solutions of various anions ( $\lambda_{\text{ex}} = 360 \text{ nm}$ ,  $\lambda_{\text{em}} = 430 \text{ nm}$ ).

For practical applications in complicated biological systems,<sup>4,61</sup> the high selectivity of a fluorescent sensor material towards the target analyte in the presence of other potentially interfering analytes is highly required. For accomplishment of this purpose, we carried out competitive fluorescence titration experiments in which the  $\text{PO}_4^{3-}$  solution was added to the suspension of **1'** (in aqueous or HEPES buffer media), which also contained the potentially competing anions. From Fig. 5 and Fig. S14–S15 (ESI<sup>†</sup>), it becomes obvious that the significant fluorescence turn-on response of the compound towards  $\text{PO}_4^{3-}$  ions is retained even in the presence of other potentially competing anions under both aqueous and physiological conditions. Therefore, the remarkable selectivity of **1'** towards  $\text{PO}_4^{3-}$  ions is retained even when other potentially interfering anions are present in the solution.

The limit of detection (LOD) of the aqueous suspension of **1'** towards  $\text{PO}_4^{3-}$  ions was determined by regulating the fluorescence emission intensity upon gradual addition of a very low concentration of the  $\text{PO}_4^{3-}$  solution to the suspension of **1'** in the aqueous medium. The plot of the fluorescence emission intensity of the aqueous suspension of **1'** against the concentration of the  $\text{PO}_4^{3-}$  solution resulted in a linear curve (Fig. S16, ESI<sup>†</sup>). The LOD value was determined according to the formula:  $\text{LOD} = 3\sigma/m$ , where  $\sigma$  represents the standard deviation

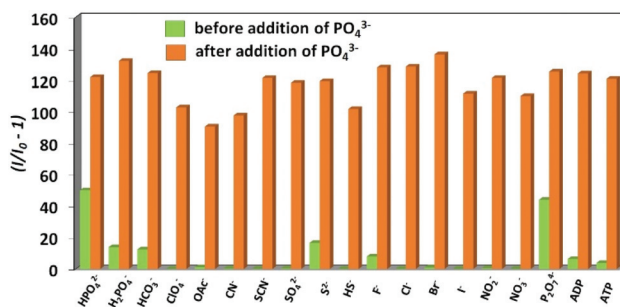


Fig. 5 Change in the fluorescence intensity of the suspension of **1'** (0.87 mM) upon the addition of 400  $\mu\text{L}$  of the 2 mM aqueous solution of  $\text{PO}_4^{3-}$  ions in the presence of 400  $\mu\text{L}$  of 2 mM aqueous solutions of other potentially competing anions ( $\lambda_{\text{ex}} = 360 \text{ nm}$ ,  $\lambda_{\text{em}} = 430 \text{ nm}$ ).

of the initial intensity of **1'** without the analyte and  $m$  corresponds to the slope of the above-stated linear curve.<sup>62</sup> The LOD value of **1'** for  $\text{PO}_4^{3-}$  sensing was estimated to be 0.196  $\mu\text{M}$  in the aqueous medium. This LOD value is lower than that of the UiO-66- $\text{NH}_2$  compound, which displayed a LOD of 1.25  $\mu\text{M}$ .<sup>30</sup>

The recyclability of the detection ability of **1'** towards  $\text{PO}_4^{3-}$  ions was investigated up to two cycles. After the first cycle of the fluorescence sensing experiment, the dispersed MOF material was collected by centrifugation, washed with copious amounts of water and finally dried in a conventional oven at 60  $^\circ\text{C}$  for 3 h. The material recovered in this way was employed in the second cycle. The compound showed an already high fluorescence intensity before the addition of the  $\text{PO}_4^{3-}$  solution in the second cycle and a very less increment in the fluorescence intensity after the addition of  $\text{PO}_4^{3-}$  in the same cycle. Thus, **1'** showed a dramatic decrease in the fluorescence turn-on response towards  $\text{PO}_4^{3-}$  detection in the second cycle (Fig. S17, ESI<sup>†</sup>). Therefore, the material displayed poor recyclability of its detection capability towards  $\text{PO}_4^{3-}$  ions in the aqueous medium.

### Mechanism for $\text{PO}_4^{3-}$ sensing

Several instrumental techniques such as FT-IR spectroscopy,  $\text{N}_2$  sorption experiment and XRPD analysis were employed to investigate the probable mechanism of  $\text{PO}_4^{3-}$  detection by the UiO-66- $\text{N}_2\text{H}_3$  material. After incubation with an aqueous solution of  $\text{PO}_4^{3-}$  ions, the compound showed broad absorption bands between 900 and 1190  $\text{cm}^{-1}$  in the IR spectrum (Fig. S4, ESI<sup>†</sup>) due to P–O stretching vibrations,<sup>63</sup> which confirmed the coordination of  $\text{PO}_4^{3-}$  ions with the framework of **1'**. This might indicate the complexation between the  $\text{PO}_4^{3-}$  ions and Zr–O clusters because the P–O bonds would limit their stretching vibrations, resulting in a decrease of their vibrational frequencies.<sup>30</sup> The symmetric stretching vibrations of the carboxylate groups in phosphate-incubated **1'** exhibited a blue shift (from 1385  $\text{cm}^{-1}$  to 1392  $\text{cm}^{-1}$ ) as compared to untreated **1'**. This might provide further evidence that  $\text{PO}_4^{3-}$  ions have a coordination effect with the Zr–O clusters and weaken the interactions between the BDC- $\text{N}_2\text{H}_3$  ligands and Zr–O clusters, thus making the carboxylate groups more free and their vibrations stronger.<sup>64</sup> Moreover, the phosphate-treated **1'** showed a BET surface area of 442  $\text{m}^2 \text{g}^{-1}$  (Fig. S9, ESI<sup>†</sup>), which is significantly lower as compared to the untreated sample (828  $\text{m}^2 \text{g}^{-1}$ ). Furthermore, **1'** was treated with phosphate in different molar ratios with respect to zirconium, and XRPD measurements were carried with these phosphate-treated samples. Upon increasing the  $\text{PO}_4^{3-} : \text{Zr}$  molar ratio, the framework of **1'** gradually collapsed (Fig. S18, ESI<sup>†</sup>) and consequently the organic linker became free. These observations indicate that the fluorescence turn-on response of **1'** upon the addition of the  $\text{PO}_4^{3-}$  solution can be attributed to the competitive coordination effect. Upon the gradual addition of the  $\text{PO}_4^{3-}$  solution, the interactions between the attached carboxylate groups and the Zr–O clusters become relatively weaker as compared to the un-treated compound. The ligand-to-metal

charge transfer (LMCT) transition from the ligand released in this way into the solution might enhance the fluorescence emission intensity.

### Effect of pH for $\text{PO}_4^{3-}$ sensing in HEPES buffer

We carried out both concentration and time-dependent  $\text{PO}_4^{3-}$  sensing experiments at four different pH (pH = 3.4, 5.4, 7.4 and 9.4) values in 10 mM HEPES buffer. The results (Fig. S19–S23, ESI†) from the concentration-dependent fluorescence sensing experiments showed that the fold increments ( $I/I_0$ ) in the fluorescence intensity for **1'** after treatment with 400  $\mu\text{L}$  of the 2 mM  $\text{PO}_4^{3-}$  solution were 6.7, 26.0, 12.7 and 0.9 at a pH of 3.4, 5.4, 7.4 and 9.4, respectively. Thus, the fold increment was the maximum at pH = 5.4 whereas the fold increment was the minimum at a highly basic pH (pH = 9.4). The fold increment increased on increasing the solution pH from 3.4 to 5.4 but it decreased at higher pH values (pH = 7.4 and 9.4). At pH = 3.4, the degree of protonation of the  $\text{PO}_4^{3-}$  ions is higher compared to that at pH = 5.4. Hence, a smaller amount of  $\text{PO}_4^{3-}$  ions is available for binding with Zr(IV) ions at pH = 3.4 than at pH = 5.4. As a result, **1'** showed a lower fold increment at pH = 3.4 compared to that at pH = 5.4. At basic pH, partial decomposition of the framework of **1'** occurs. Moreover, in a basic medium, the  $-\text{NH}$  proton of the hydrazinyl group can be deprotonated.<sup>65</sup> As a result, **1'** showed a high fluorescence intensity at basic pH, even before the addition of the  $\text{PO}_4^{3-}$  solution. Therefore, the fold increment in the fluorescence intensity decreased with the increment in pH from 7.4 to 9.4.

The saturation times (*i.e.*, time to reach the saturation point in fluorescence intensity after the addition of 400  $\mu\text{L}$  of the 2 mM  $\text{PO}_4^{3-}$  solution) were 45, 75, 100 and 5 min at a pH of 3.4, 5.4, 7.4 and 9.4, respectively (Fig. S11 and S24–S26, ESI†). With increasing pH, the saturation time increased up to pH = 7.4. At pH = 9.4, **1'** was already in a highly fluorescent state, even before the addition of the  $\text{PO}_4^{3-}$  solution. Therefore, the fluorescence intensity of **1'** did not increase significantly with time after the addition of the  $\text{PO}_4^{3-}$  solution at pH = 9.4.

### $\text{PO}_4^{3-}$ sensing in real samples

As compound **1'** is highly sensitive towards  $\text{PO}_4^{3-}$  ions in aqueous as well as in the HEPES medium, we decided to perform the sensing experiments with real biological and environmental samples. For this purpose, we chose a total of six samples of three different types (water, human urine and human blood serum). We spiked each of these samples with known concentrations of the  $\text{PO}_4^{3-}$  solution. Then, we treated the MOF probe with these spiked samples and recorded the fluorescence spectra after 90 min. After the spiked-and-recovery experiments, the amount of  $\text{PO}_4^{3-}$  ions found and the recovery percentages are summarized in Table 1. In the case of all the samples, excellent recovery percentages and low RSD values make probe **1'** a smart candidate for quantifying the  $\text{PO}_4^{3-}$  concentration present in different real and complicated biological as well as environmental samples.

**Table 1** Detection performance of **1'** for  $\text{PO}_4^{3-}$  ions in real water, human urine and human blood serum samples

Sample name	$\text{Na}_3\text{PO}_4$ spiked ( $\mu\text{M}$ )	$\text{Na}_3\text{PO}_4$ found <sup>a</sup> ( $\mu\text{M}$ )	Recovery (%)
Tap water	0	5.30 $\pm$ 0.75	NA
	10	8.72 $\pm$ 0.91	87.20
	20	19.62 $\pm$ 1.93	98.10
	30	29.66 $\pm$ 1.18	98.87
Lake water	0	5.74 $\pm$ 0.69	NA
	10	9.18 $\pm$ 3.92	91.80
	20	20.08 $\pm$ 0.15	100.40
	30	29.23 $\pm$ 0.61	97.43
Human urine 1	0	58.21 $\pm$ 1.44	NA
	10	9.78 $\pm$ 3.27	97.80
	20	19.56 $\pm$ 1.53	97.80
	30	29.52 $\pm$ 0.92	98.40
Human urine 2	0	63.73 $\pm$ 0.59	NA
	10	9.80 $\pm$ 1.73	98.00
	20	19.68 $\pm$ 1.42	98.40
	30	29.57 $\pm$ 1.21	98.57
Human blood serum 1	0	34.58 $\pm$ 0.12	NA
	10	9.73 $\pm$ 0.62	97.30
	20	19.30 $\pm$ 0.72	96.50
	30	28.42 $\pm$ 0.45	94.73
Human blood serum 2	0	35.98 $\pm$ 1.63	NA
	10	9.55 $\pm$ 1.98	95.5
	20	19.57 $\pm$ 1.33	97.85
	30	28.36 $\pm$ 1.13	94.53

<sup>a</sup>  $\text{Na}_2\text{S}$  found  $\pm$  RSD ( $n = 3$ ).

### Intracellular $\text{PO}_4^{3-}$ sensing

Before performing the live cell imaging experiment for  $\text{PO}_4^{3-}$  ions, we checked the particle size of **1'** by FE-SEM. Fig. S27 (ESI†) reveals that **1'** has an average particle size of less than 100 nm. Thus, its particles can easily penetrate through the cell membrane.

The intrinsic phosphate species (inorganic phosphate and other phosphorylated derivatives) varies among different cell types and may correlate strongly with metabolism and the energy status.<sup>66,67</sup> To check the potential of **1'** to perform intracellular phosphate detection, fluorescence imaging experiments were performed in macrophage J774A.1, cervical cancer HeLa and glioblastoma U87MG cells. The unlabeled cells were healthy and they did not exhibit any blue fluorescence (Fig. 6a, g and m). Macrophage J774A.1 cells loaded with the probe (Fig. 6d, J774 panel) were healthy and exhibited blue fluorescence (Fig. 6e, J774 panel). The superposition of the phase and fluorescence indicates that the signal arises from the cells (Fig. 6f, J774 panel, superimposed). HeLa cancer cells loaded with the probe showed a distorted cellular morphology but this could be due to the uptake of the suspension of the probe (Fig. 6g and j, HeLa panel). These cells exhibited intense bright blue fluorescence (Fig. 6h and k, HeLa panel, fluorescence). The superposition of the phase and fluorescence indicates that the signal arises from the cells (Fig. 6i and l, HeLa panel, superimposed). The probe loaded glioblastoma U87MG cells displayed strong fluorescence signals (Fig. 6n and q, HeLa panel, fluorescence), and the superposition of the phase and fluorescence indicates that the signal stems from

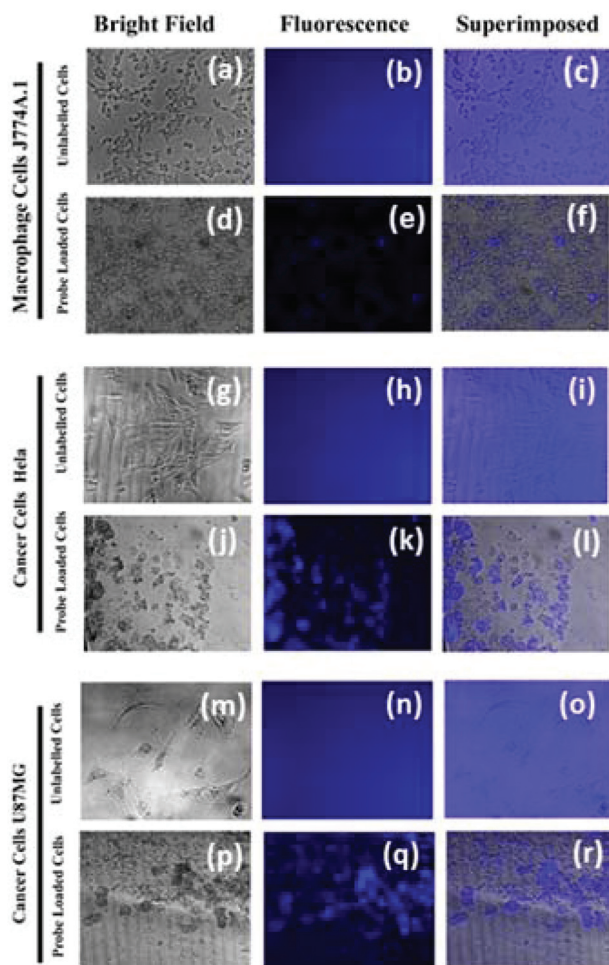


**Fig. 6** Three different types of cells, macrophage J774A.1 (J774 panel), cervical cancer HeLa (HeLa panel) and glioblastoma U87MG (U87MG panel) were either as such (a, b, g, h, m, n) or loaded with probe **1'** (d, j, p). Probe loaded cells exhibited bright blue fluorescence (e, k, q) and superposition of the bright field (c, i, o) and fluorescence (f, l, r) indicates that the signal arises from the cells associated with the probe ( $\lambda_{\text{ex}} = 390 \text{ nm}$ ,  $\lambda_{\text{em}} = 430 \text{ nm}$ ).

the cells (Fig. 6o and r, U87MG panel, superimposed). The comparison of fluorescence in all three cells indicates that the fluorescence signal is more in HeLa and U87MG cells compared to the J774A.1 cells. This difference in fluorescence could be due to the inherent difference in their intracellular total phosphate level<sup>68–70</sup> or because of the differential levels of stress inside the dissimilar cells owing to probe loading. Overall, probe **1'** has the potential to detect intracellular phosphate and it also has the potential to show difference in the intracellular phosphate level.

#### Sensing behaviour towards 4-NB

The fluorescence emission spectra of **1'** (Fig. S28, ESI<sup>†</sup>) were recorded in water as well as various organic solvents such as acetonitrile, methanol, ethanol, toluene, DMF and dimethylsulphoxide (DMSO).<sup>71</sup> Among the different solvents tested, **1'** showed the highest fluorescence emission intensity in DMSO.

The compound also exhibited a high fluorescence intensity in DMSO/HEPES (10 mM, pH = 7.4) buffer (v/v = 9 : 1) (Fig. S28, ESI<sup>†</sup>). Furthermore, the compound showed outstanding selectivity towards 4-NB over other aldehydes in the DMSO/HEPES buffer (v/v = 9 : 1) medium. Therefore, this solvent mixture was chosen as the medium for preparing the suspension of **1'** in order to perform the sensing experiments for 4-NB.

In order to determine the potential of Zr-UiO-66-N<sub>2</sub>H<sub>3</sub> as a fluorogenic sensor for 4-NB detection, fluorescence titration experiments were performed with the suspension of **1'** in the DMSO/HEPES (9 : 1, v/v) mixture, even in the presence of potentially competitive aldehydes. The fluorescence emission ( $\lambda_{\text{ex}} = 360 \text{ nm}$ ) spectra of the suspension of **1'** were recorded in the range of 385–585 nm upon gradual addition (50  $\mu\text{L}$  for each addition) of the 50 mM 4-NB solution. The fluorescence emission intensities were regulated at 430 nm. As shown in Fig. 7, the saturation of the fluorescence intensity was observed after the addition of 400  $\mu\text{L}$  of the 50 mM 4-NB solution. Further addition of the 4-NB solution did not result in any considerable decrease in the fluorescence intensity.

For real-world applications of the sensor material, its high selectivity for 4-NB over other potentially competing aldehydes is highly required. Therefore, the fluorescence turn-off responses of **1'** towards various other aldehydes were recorded including formaldehyde, benzaldehyde, acetaldehyde, 4-chlorobenzaldehyde, valeraldehyde, butyraldehyde, crotonaldehyde, anisaldehyde, propionaldehyde, 2-nitrobenzaldehyde (2-NB) and 3-nitrobenzaldehyde (3-NB). As shown in Fig. 8, the addition of the 4-NB solution to the suspension of **1'** in the DMSO/HEPES mixture resulted in a dramatic decrease (quenching efficiency = 92%) in the fluorescence emission intensity. The fluorescence quenching efficiencies of all other potentially competing aldehydes were relatively less as compared to that of 4-NB (Fig. S29, ESI<sup>†</sup>). Hence, it can be con-

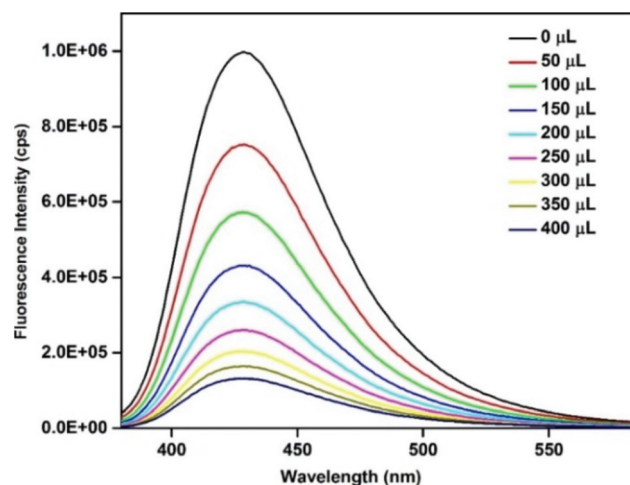


**Fig. 7** Quenching of the fluorescence intensity of **1'** (0.87 mM) by incremental addition of 400  $\mu\text{L}$  of the 50 mM 4-NB solution to a 3 mL stable suspension of **1'** in HEPES/DMSO (9 : 1, v/v) ( $\lambda_{\text{ex}} = 360 \text{ nm}$ ,  $\lambda_{\text{em}} = 430 \text{ nm}$ ).

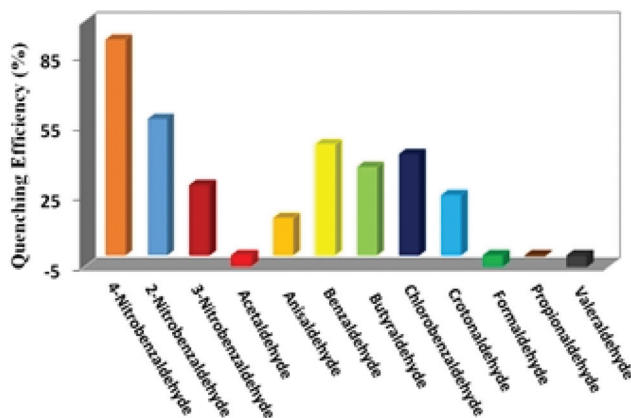


Fig. 8 Fluorescence quenching efficiencies of different aldehydes towards **1'** (0.87 mM) in the DMSO/HEPES (9 : 1, v/v) mixture. The fluorescence spectra were recorded after the addition of 400  $\mu$ L of 50 mM aldehyde solutions ( $\lambda_{\text{ex}} = 360$  nm,  $\lambda_{\text{em}} = 430$  nm).

cluded that **1'** is highly selective towards 4-NB over other potentially intrusive aldehydes in the DMSO/HEPES mixture.

A fluorescent probe must show high selectivity towards the target analyte in the presence of other possibly competing analytes, which is highly required for the practical applications of a fluorescent sensor material in complex biological media.<sup>72,73</sup> In order to fulfil this purpose, we carried out competitive fluorescence titration experiments in which the 4-NB solution was added to the suspension of **1'**, which also contained the possibly competing aldehydes. It is obvious from Fig. 9 and Fig. S30 (ESI<sup>†</sup>) that the outstanding fluorescence quenching efficiency of the compound towards 4-NB was retained even in the presence of other possibly interfering aldehydes in the DMSO/HEPES mixture. Hence, the compound showed remarkable selectivity towards 4-NB, even in the presence of other potentially interfering aldehydes.

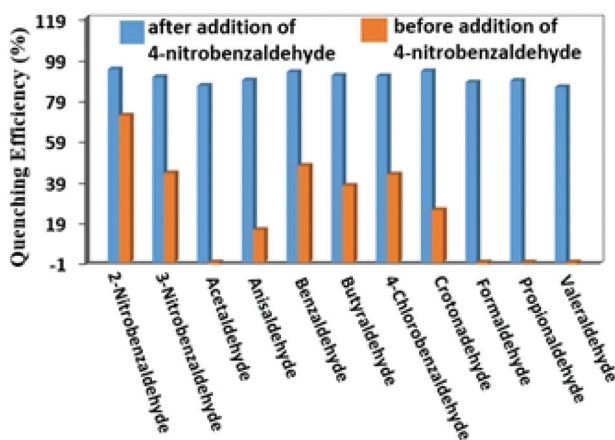


Fig. 9 Change in the fluorescence intensity of the suspension of **1'** (0.87 mM) (DMSO/HEPES (9 : 1, v/v)) upon the addition of 400  $\mu$ L of the 50 mM 4-NB solution in the presence of 400  $\mu$ L of 50 mM solutions of other potentially competing aldehydes ( $\lambda_{\text{ex}} = 360$  nm,  $\lambda_{\text{em}} = 430$  nm).

The limit of detection (LOD) of **1'** for 4-NB was evaluated by regulating the fluorescence emission intensity of the compound upon gradual addition of very low concentrations of the 4-NB solution in the DMSO/HEPES (9 : 1, v/v) mixture. A linear curve (Fig. S31, ESI<sup>†</sup>) was achieved when the fluorescence intensity of **1'** was plotted against the concentration of the 4-NB solution. The LOD value was estimated by using the formula:  $\text{LOD} = 3\sigma/m$ , where  $\sigma$  is the standard deviation of the initial intensity of **1'** without the analyte and  $m$  denotes the slope of the above-stated linear curve.<sup>62</sup> The LOD value of **1'** for 4-NB was found to be 4.7  $\mu$ M.

For checking the recyclability of the detection capability of **1'** towards 4-NB, fluorescence sensing experiments were carried out up to four cycles. The compound was collected by centrifugation after each cycle of the fluorescence sensing measurement. Then, it was washed with a sufficient amount of acetone and finally dried in a conventional oven at 70  $^{\circ}$ C for 30 min. After the first cycle, the fluorescence emission intensity of **1'** decreased significantly. However, there was no considerable decrease in the fluorescence emission intensity after the subsequent cycles. Therefore, the fluorescence quenching efficiency of the compound decreased considerably in the second cycle, although it remained almost unaltered in the later cycles (Fig. S32, ESI<sup>†</sup>). Therefore, **1'** exhibited partial recyclability of its detection performance towards 4-NB.

For determination of the nature of the quenching (static versus dynamic) process, we analyzed the fluorescence quenching data by using the Stern–Volmer (S–V) equation which is shown below: towards 4-NB.

$$(I_0/I) = K_{\text{sv}} [A] + 1$$

where  $I_0$  and  $I$  denote the fluorescence intensities of **1'** in the absence and presence of the analyte, respectively,  $[A]$  corresponds to the molar concentration of the analyte, and  $K_{\text{sv}}$  represents the quenching constant.<sup>71</sup> In Fig. S33 (ESI<sup>†</sup>), the S–V plot for quenching the fluorescence intensity of **1'** by 4-NB is shown. The value of  $K_{\text{sv}}$  for 4-NB, which was determined from this plot, was found to be  $0.59 \times 10^4 \text{ M}^{-1}$ . The S–V plot is linear in nature in the lower concentration range of 4-NB, although it shows non-linearity in the higher concentration range. These results suggest that either a static or dynamic quenching process occurs in this system.<sup>62,71,74,75</sup>

### Mechanism for the sensing of 4-NB

It is very well known that amine compounds form imines upon condensation with aldehyde compounds. All the aldehydes are supposed to form imine bonds with the  $-\text{NHNH}_2$  moiety attached to the BDC- $\text{NHNH}_2$  ligand. Among all the selected aldehydes, the electron-withdrawing effect of 4-NB upon imine formation will be higher as compared to the others due to the long conjugation of the imine group with the electron-withdrawing nitro group at the *para* position. As a result, the nitro group of 4-NB reduces the electron density from the imine group much more than the other aldehydes. Hence, the electron density in the BDC- $\text{NHNH}_2$  ligand is reduced to a larger extent for 4-NB as compared to the other

aldehydes. Therefore, the highest fluorescence quenching effect is observed for 4-NB among all the chosen aldehydes.<sup>76,77</sup>

In order to prove the proposed sensing mechanism, we performed FT-IR spectroscopy, mass spectrometry and time-resolved photoluminescence lifetime experiments. In the FT-IR spectrum of untreated **1'** there is no peak at around 1630 cm<sup>-1</sup> whereas there is a new peak at 1637 cm<sup>-1</sup> in the IR spectrum of **1'** treated with 4-NB (Fig. S4, ESI†). This peak corresponds to the imine bond formed between the hydrazine group of the BDC-N<sub>2</sub>H<sub>3</sub> ligand and the aldehyde group of 4-NB. In the mass spectrum of **1'** (without the treatment of 4-NB), (Fig. S34, ESI†) there is a peak at (+ESI) *m/z* = 195.0497, whereas 4-NB treated **1'** (Fig. S35, ESI†) showed a peak at (+ESI) *m/z* = 328.0631, which corresponds to (*E*)-2-(2-(4-nitrobenzylidene)hydrazinyl) terephthalic acid. This observation confirms that there is an imine product formed by the condensation reaction between the hydrazine functionalized BDC ligand and 4-NB. Hence, from FT-IR spectroscopy and mass spectrometry, it can be confirmed that the reaction of **1'** with 4-NB forms an imine compound.

The two quenching mechanisms (static and dynamic) can be differentiated by studying the time-resolved fluorescence experiments of the luminescence decay of the fluorophore compound at different concentrations of the quencher. If the fluorescence lifetime of the sensor material decreases, the quenching process is considered as dynamic because additional relaxation of the excited-state lifetime in this process results from the collision with the quencher. If the fluorescence lifetime of the sensor material does not change after increasing the addition of the quencher, it is regarded as a static quenching process.<sup>75,78,79</sup> Fig. S36 (ESI†) represents the lifetime decay profile of **1'** before and after the addition of 400 μL of the 50 mM 4-NB solution. As shown in Table S2, ESI†, the average excited-state lifetimes ( $\langle\tau\rangle^*$ ) of **1'** are 2.70 and 1.52 ns before and after the addition of 400 μL of the 50 mM 4-NB solution, respectively. Hence, it can be concluded that the fluorescence quenching mechanism in this system is mainly static in nature.

### Similarities and dissimilarities between PO<sub>4</sub><sup>3-</sup> and 4-NB sensing

The similarity (Table S3, ESI†) between PO<sub>4</sub><sup>3-</sup> and 4-NB sensing involves the high selectivity of **1'** towards PO<sub>4</sub><sup>3-</sup> and 4-NB even in the presence of potentially competitive analytes.

The dissimilarities (Table S3, ESI†) observed between the sensing of PO<sub>4</sub><sup>3-</sup> and 4-NB involve the sensing medium, the nature of fluorescence change, response time, sensing mechanism and LOD values. We have chosen water or HEPES buffer (10 mM, pH = 7.4) as the medium for PO<sub>4</sub><sup>3-</sup> sensing because the PO<sub>4</sub><sup>3-</sup> ion is highly soluble in these two liquids and it is highly abundant in environmental water samples. Moreover, HEPES buffer (pH = 7.4) is known to mimic the physiological conditions. On the other side, 4-NB sensing was carried out in a DMSO/HEPES mixture because 4-NB is not soluble in pure HEPES buffer and hence DMSO was used to increase its solubi-

lity. Either an increase or decrease in fluorescence intensity was observed for PO<sub>4</sub><sup>3-</sup> and 4-NB sensing, respectively. The mechanism for PO<sub>4</sub><sup>3-</sup> sensing involves its coordination with the Zr(IV) ions causing partial collapse of the framework and subsequent slow release of ligand molecules. For 4-NB sensing, the -NHNH<sub>2</sub> group of the ligand directly forms a covalent imine bond with the -CHO group of 4-NB. As a result, the response time for PO<sub>4</sub><sup>3-</sup> sensing is relatively longer compared to 4-NB detection. The LOD values for PO<sub>4</sub><sup>3-</sup> and 4-NB sensing were 0.2 and 4.7 μM, respectively.

## Conclusions

We have successfully synthesized and characterized a hydrazine-functionalized Zr(IV) MOF material **1**, which has the UiO-66 framework topology. The compound was synthesized by heating a mixture of ZrOCl<sub>2</sub>·8H<sub>2</sub>O, H<sub>2</sub>BDC-N<sub>2</sub>H<sub>3</sub> ligand and benzoic acid (ZrOCl<sub>2</sub>·8H<sub>2</sub>O/BDC-N<sub>2</sub>H<sub>3</sub>/benzoic acid molar ratio = 1 : 1 : 30) in DMF at 120 °C for 24 h. The activated compound (**1'**) showed moderate thermal stability up to 400 °C. It retained its crystallinity and hence structural robustness when exposed to water, acetic acid and 1M HCl solutions. As verified by the N<sub>2</sub> sorption experiments, the specific BET surface area of **1'** is 818 m<sup>2</sup> g<sup>-1</sup>. We have employed **1'** as a fluorescent turn-on probe for the selective detection of phosphate (both *in vivo* and *in vitro*) and also as a fluorescent turn-off probe for the selective sensing of 4-NB in the DMSO/HEPES (9 : 1, v/v) medium. Even in the presence of interfering intrusive species, the probe retains its high selectivity. The probe also features high sensitivity. Its detection limits for PO<sub>4</sub><sup>3-</sup> ions and 4-NB are 0.196 and 4.7 μM, respectively. Probe **1'** is able to detect phosphate in living cells. It can also respond towards the difference in the intracellular phosphate level. The MOF probe can be used efficiently for determining PO<sub>4</sub><sup>3-</sup> ions in real samples such as tap water, lake water, human urine and human blood serum. Furthermore, it can be utilized for the *in vitro* detection of 4-NB in the fluid secreted from eyes upon exposure to sunlight after applying the chloramphenicol eye-drop.

## Conflicts of interest

There are no conflicts to declare.

## Acknowledgements

The authors express their gratitude towards the Science and Engineering Research Board (SERB; grant no. EEQ/2016/000012), New Delhi for financial support.

## Notes and references

- 1 W.-L. Cheng, J.-W. Sue, W.-C. Chen, J.-L. Chang and J.-M. Zen, *Anal. Chem.*, 2010, **82**, 1157–1161.

- 2 K.-Y. A. Lin, S.-Y. Chen and A. P. Jochems, *Mater. Chem. Phys.*, 2015, **160**, 168–176.
- 3 C. Warwick, A. Guerreiro and A. Soares, *Biosens. Bioelectron.*, 2013, **41**, 1–11.
- 4 C. Dai, C.-X. Yang and X.-P. Yan, *Anal. Chem.*, 2015, **87**, 11455–11459.
- 5 G. M. J. B. V. Henegouwen, *J. Photochem. Photobiol., B*, 1991, **10**, 183–210.
- 6 H. Bauer and S. M. Rosenthal, *J. Am. Chem. Soc.*, 1944, **66**, 611–614.
- 7 H. Lowry, N. J. Rosebrough, A. L. Farr and R. J. Randall, *J. Biol. Chem.*, 1951, **193**, 265–275.
- 8 O. M. Yaghi, M. O’Keeffe, N. W. Ockwig, H. K. Chae, M. Eddaoudi and J. Kim, *Nature*, 2003, **423**, 705–714.
- 9 S. Kitagawa, R. Kitaura and S. Noro, *Angew. Chem., Int. Ed.*, 2004, **43**, 2334–2375.
- 10 G. Férey, *Chem. Soc. Rev.*, 2008, **37**, 191–214.
- 11 J. Lee, O. K. Farha, J. Roberts, K. A. Scheidt, S. T. Nguyen and J. T. Hupp, *Chem. Soc. Rev.*, 2009, **38**, 1450–1459.
- 12 L. Ma, C. Abney and W. Lin, *Chem. Soc. Rev.*, 2009, **38**, 1248–1256.
- 13 D. Banerjee, A. J. Cairns, J. Liu, R. K. Motkuri, S. K. Nune, C. A. Fernandez, R. Krishna, D. M. Strachan and P. K. Thallapally, *Acc. Chem. Res.*, 2015, **48**, 211–219.
- 14 J. Liu, Y. Wei, P. Li, Y. Zhao and R. Zou, *J. Phys. Chem. C*, 2017, **121**, 13249–13255.
- 15 C. Orellana-Tavra, R. J. Marshall, E. F. Baxter, I. A. Lázaro, A. Tao, A. K. Cheetham, R. S. Forgan and D. Fairen-Jimenez, *J. Mater. Chem. B*, 2016, **4**, 7697–7707.
- 16 S. Rojas, F. J. Carmona, C. R. Maldonado, P. Horcajada, T. Hidalgo, C. Serre, J. A. R. Navarro and E. Barea, *Inorg. Chem.*, 2016, **55**, 2650–2663.
- 17 E. Gkaniatsou, C. Sicard, R. Ricoux, J.-P. Mahy, N. Steunou and C. Serre, *Mater. Horiz.*, 2017, **4**, 55–63.
- 18 M. B. Majewski, A. J. Howarth, P. Li, M. R. Wasielewski, J. T. Hupp and O. K. Farha, *CrystEngComm*, 2017, **19**, 4082–4091.
- 19 D. Feng, T.-F. Liu, J. Su, M. Bosch, Z. Wei, W. Wan, D. Yuan, Y.-P. Chen, X. Wang, K. Wang, X. Lian, Z.-Y. Gu, J. Park, X. Zou and H.-C. Zhou, *Nat. Commun.*, 2015, **6**, 5979–5987.
- 20 R. Dalapati, B. Sakthivel, M. K. Ghosal, A. Dhakshinamoorthy and S. Biswas, *CrystEngComm*, 2017, **19**, 5915–5925.
- 21 S. Sen, N. N. Nair, T. Yamada, H. Kitagawa and P. K. Bharadwaj, *J. Am. Chem. Soc.*, 2012, **134**, 19432–19437.
- 22 S. Nandi, H. Reinsch, S. Banesh, N. Stock, V. Trivedi and S. Biswas, *Dalton Trans.*, 2017, **46**, 12856–12864.
- 23 S. S. Nagarkar, T. Saha, A. V. Desai, P. Talukdar and S. K. Ghosh, *Sci. Rep.*, 2014, **4**, 7053–7058.
- 24 M. Kandiah, M. H. Nilsen, S. Usseglio, S. Jakobsen, U. Olsbye, M. Tilset, C. Larabi, E. A. Quadrelli, F. Bonino and K. P. Lillerud, *Chem. Mater.*, 2010, **22**, 6632–6640.
- 25 X. Liu, N. K. Demir, Z. Wu and K. Li, *J. Am. Chem. Soc.*, 2015, **137**, 6999–7002.
- 26 B. V. D. Voorde, I. Stassen, B. Bueken, F. Vermoortele, D. D. Vos, R. Ameloot, J.-C. Tan and T. D. Bennett, *J. Mater. Chem. A*, 2015, **3**, 1737–1742.
- 27 M. L. Pinto, S. Dias and J. O. Pires, *ACS Appl. Mater. Interfaces*, 2013, **5**, 2360–2363.
- 28 Z. Wang, H. Ren, S. Zhang, F. Zhang and J. Jin, *J. Mater. Chem. A*, 2017, **5**, 10968–10977.
- 29 D. J. Tranchemontagne, J. L. Mendoza-Cortés, M. O’Keeffe and O. M. Yaghi, *Chem. Soc. Rev.*, 2009, **38**, 1257–1283.
- 30 J. Yang, Y. Dai, X. Zhu, Z. Wang, Y. Li, Q. Zhuang, J. Shi and J. Gu, *J. Mater. Chem. A*, 2015, **3**, 7445–7452.
- 31 G.-Y. Wang, C. Song, D.-M. Kong, W.-J. Ruan, Z. Chang and Y. Li, *J. Mater. Chem. A*, 2014, **2**, 2213–2220.
- 32 B. Gole, A. K. Bar and P. S. Mukherjee, *Chem. Commun.*, 2011, **47**, 12137–12139.
- 33 S. Okorochenkova, K. Burglova, I. Popa and J. Hlavac, *Org. Lett.*, 2015, **17**, 180–183.
- 34 S. J. Deka, A. Roy, V. Ramakrishnan, D. Manna and V. Trivedi, *Chem. Biol. Drug Des.*, 2017, **89**, 953–963.
- 35 R. Deshmukh and V. Trivedi, *PLoS One*, 2014, **9**, e103706.
- 36 B. Muthuraj, S. Layek, S. N. Balaji, V. Trivedi and P. K. Iyer, *ACS Chem. Neurosci.*, 2015, **6**, 1880–1891.
- 37 N. Stock and S. Biswas, *Chem. Rev.*, 2012, **112**, 933–969.
- 38 A. Buragohain and S. Biswas, *CrystEngComm*, 2016, **18**, 4374–4381.
- 39 R. Dalapati, S. N. Balaji, V. Trivedi, L. Khamari and S. Biswas, *Sens. Actuators, B*, 2017, **245**, 1039–1049.
- 40 A. Schaate, P. Roy, A. Godt, J. Lippke, F. Waltz, M. Wiebecke and P. Behrens, *Chem. – Eur. J.*, 2011, **17**, 6643–6651.
- 41 J. H. Cavka, S. Jakobsen, U. Olsbye, N. Guillou, C. Lamberti, S. Bordiga and K. P. Lillerud, *J. Am. Chem. Soc.*, 2008, **130**, 13850–13851.
- 42 L. Valenzano, B. Civalleri, S. Chavan, S. Bordiga, M. H. Nilsen, S. Jakobsen, K. P. Lillerud and C. Lamberti, *Chem. Mater.*, 2011, **23**, 1700–1718.
- 43 M. R. Destefano, T. Islamoglu, S. J. Garibay, J. T. Hupp and O. K. Farha, *Chem. Mater.*, 2017, **29**, 1357–1361.
- 44 D. Cunha, C. Gaudin, I. Colinet, P. Horcajada, G. Maurin and C. Serre, *J. Mater. Chem. B*, 2013, **1**, 1101–1108.
- 45 Y. Luan, Y. Qi, Z. Jin, X. Peng, H. Gao and G. Wang, *RSC Adv.*, 2015, **5**, 19273–19278.
- 46 X. Du, Y. Luan, F. Yang, D. Ramella and X. Shu, *New J. Chem.*, 2017, **41**, 4400–4405.
- 47 A. J. Howarth, Y. Liu, P. Li, Z. Li, T. C. Wang, J. T. Hupp and O. K. Farha, *Nat. Rev. Mater.*, 2016, **1**, 1–15.
- 48 M. J. Katz, Z. J. Brown, Y. J. Colón, P. W. Siu, K. A. Scheidt, R. Q. Snurr, J. T. Hupp and O. K. Farha, *Chem. Commun.*, 2013, **49**, 9449–9451.
- 49 S. J. Garibay and S. M. Cohen, *Chem. Commun.*, 2010, **46**, 7700–7702.
- 50 M. Kim, S. J. Garibay and S. M. Cohen, *Inorg. Chem.*, 2011, **50**, 729–731.
- 51 Y. Dong, H. Zhang, F. Lei, M. Liang, X. Qian, P. Shen, H. Xu, Z. Chen, J. Gao and J. Yao, *J. Solid State Chem.*, 2017, **245**, 160–163.

- 52 I. Ahmed, N. A. Khan and S. H. Jhung, *Chem. Eng. J.*, 2017, **321**, 40–47.
- 53 R. Dalapati, B. Sakthivel, A. Dhakshinamoorthy, A. Buragohain, A. Bhunia, C. Janiak and S. Biswas, *CrystEngComm*, 2016, **18**, 7855–7864.
- 54 F. Ragon, B. Campo, Q. Yang, C. Martineau, A. D. Wiersum, A. Lago, V. Guillerme, C. Hemsley, J. F. Eubank, M. Vishnuvarthan, F. Taulelle, P. Horcajada, A. Vimont, P. L. Llewellyn, M. Daturi, S. Devautour-Vinot, G. Maurin, C. Serre, T. Devic and G. Clet, *J. Mater. Chem. A*, 2015, **3**, 3294–3309.
- 55 L. Shen, R. Liang, M. Luo, F. Jing and L. Wu, *Phys. Chem. Chem. Phys.*, 2015, **17**, 117–121.
- 56 G.-Y. Wang, C. Song, D.-M. Kong, W.-J. Ruan, Z. Chang and Y. Li, *J. Mater. Chem. A*, 2014, **2**, 2213–2220.
- 57 X.-C. Yi, M.-X. Huang, Y. Qi and E.-Q. Gao, *Dalton Trans.*, 2014, **43**, 3691–3697.
- 58 S. Wang, J. Wang, W. Cheng, X. Yang, Z. Zhang, Y. Xu, H. Liu, Y. Wu and M. Fang, *Dalton Trans.*, 2015, **44**, 8049–8061.
- 59 K. S. Asha, K. Bhattacharyya and S. Mandal, *J. Mater. Chem. C*, 2014, **2**, 10073–10081.
- 60 Z.-Z. Lu, R. Zhang, Y.-Z. Li, Z.-J. Guo and H.-G. Zheng, *J. Am. Chem. Soc.*, 2011, **133**, 4172–4174.
- 61 P. A. Jr, Y. Liu, M. A. Palacios, T. Minami, Z. Wang and R. Nishiyabu, *Chem. – Eur. J.*, 2013, **19**, 8497–8506.
- 62 A. Das and S. Biswas, *Sens. Actuators, B*, 2017, **250**, 121–131.
- 63 C. Luengo, M. Brigante, J. Antelo and M. Avena, *J. Colloid Interface Sci.*, 2006, **300**, 511–518.
- 64 X. Zhu, J. Gu, Y. Wang, B. Li, Y. Li, W. Zhao and J. Shi, *Chem. Commun.*, 2014, **50**, 8779–8782.
- 65 R. Dalapati, S. Nandi, H. Reinsch, B. K. Bhunia, B. B. Mandal, N. Stock and S. Biswas, *CrystEngComm*, 2018, **20**, 4194–4201.
- 66 B. L. Foster, K. A. Tompkins, R. B. Rutherford, H. Zhang, E. Y. Chu, H. Fong and M. J. Somerman, *Birth Defects Res., Part C*, 2008, **84**, 281–314.
- 67 A. H. Malik, S. Hussain, A. S. Tanwar, S. Layek, V. Trivedi and P. K. Iyer, *Analyst*, 2015, **140**, 4388–4392.
- 68 M. Nakajima, M. Nagahashi, O. M. Rashid, K. Takabe and T. Wakai, *Tumor Biol.*, 2017, **39**, 1–9.
- 69 A. Maiti, K. Takabe and N. C. Hait, *Cell. Signalling*, 2017, **32**, 85–92.
- 70 L. E. Guo, J. F. Zhang, X. Y. Liu, L. M. Zhang, H. L. Zhang, J. H. Chen, X. G. Xie, Y. Zhou, K. Luo and J. Yoon, *Anal. Chem.*, 2015, **87**, 1196–1201.
- 71 A. Buragohain, M. Yousufuddin, M. Sarma and S. Biswas, *Cryst. Growth Des.*, 2016, **16**, 842–851.
- 72 F. V. Mansano, R. M. A. Kazaoka, G. E. Ronsein, F. M. Prado, T. C. Genaro-Mattos, M. Uemi, P. D. Mascio and S. Miyamoto, *Anal. Chem.*, 2010, **82**, 6775–6781.
- 73 M. Li, L. Shi, T. Xie, C. Jing, G. Xiu and Y.-T. Long, *ACS Sens.*, 2017, **2**, 263–267.
- 74 M. SK and S. Biswas, *CrystEngComm*, 2016, **18**, 3104–3113.
- 75 X. Sun, Y. Wang and Y. Lei, *Chem. Soc. Rev.*, 2015, **44**, 8019–8061.
- 76 M. Ganguly, J. Pal, C. Mondal, A. Pal and T. Pal, *Dalton Trans.*, 2015, **44**, 4370–4379.
- 77 K. Ngamdee, S. Martwiset, T. Tuntulani and W. Ngeonte, *Sens. Actuators, B*, 2012, **173**, 682–691.
- 78 A. Ueno, I. Suzuki and T. Osa, *J. Am. Chem. Soc.*, 1989, **111**, 6391–6397.
- 79 A.-Q. Gong and X.-S. Zhu, *J. Pharm. Anal.*, 2013, **3**, 415–420.